CHIN. PHYS. LETT. Vol. 38, No. 8 (2021) 085201

Excitation of RSAEs during Sawteeth-Like Oscillation in EAST

Ming Xu(徐明)[1], Guoqiang Zhong(钟国强)[1*], Baolong Hao(郝保龙)[2], Wei Shen(申伟)[1], Liqun Hu(胡立群)[1], Wei Chen(陈伟)[3], Zhiyong Qiu(仇志勇)[4], Xuexi Zhang(张学习)[1], Youjun Hu(胡友俊)[1], Yingying Li(李颖颖)[1,5,6], Hailin Zhao(赵海林)[1], Haiqing Liu(刘海庆)[1], Bo Lyu(吕波)[1], and the EAST Team[1]

[1]*Institute of Plasma Physics, Chinese Academy of Sciences (ASIPP), Hefei 230031, China*
[2]*Advanced Energy Research Center, Shenzhen University, Shenzhen 518060, China*
[3]*Southwestern Institute of Physics, Chengdu 610041, China*
[4]*Department of Physics, Zhejiang University, Hangzhou 310027, China*
[5]*Enn Science and Technology Development Co., Ltd, Langfang 065001, China*
[6]*Hebei Key Laboratory of Compact Fusion, Langfang 065001, China*

(Received 9 March 2021; accepted 8 July 2021; published online 2 August 2021)

The excitation condition of reversed shear Alfvén eigenmodes (RSAEs) has been investigated during sawtooth-like oscillation in the EAST tokamak. The sawtooth-like phenomena can be reproduced in the configuration of reversed magnetic shear, and the threshold gradient of electron temperature is formed accordingly, together with the increasing of the confinement of thermal particles. The distribution function of energetic ions density is altered dramatically when the neutral beam is switched from NBI1L (tangent) to NBI1R (perpendicular), which can be captured by the measurement of radial neutron camera. The RSAEs are excited easily in the vicinity of $q_{\min}$ ($1.99\,\mathrm{m} \leq R \leq 2.06\,\mathrm{m}$) for the injection of neutral beam with perpendicular direction, which should be excited by the steep gradient of energetic ions density. Furthermore, the excitation of RSAEs and the formation of threshold gradient of electron temperature can take place concurrently, which means that the neutral beam with perpendicular injection is beneficial for the establishment of internal transport barrier.

DOI: 10.1088/0256-307X/38/8/085201

The development of plasma scenarios with internal transport barriers (ITBs)[1] and reversed magnetic shear (RMS)[2,3] are promising for future tokamak devices. The Alfvén eigenmodes are easily excited when the distribution function of energetic ions density is suitable,[4] e.g., the reversed shear Alfvén eigenmodes (RSAEs)[5–8] can be excited in the configuration of RMS. Furthermore, double tearing modes (DTMs)[9–11] can be excited under the configuration of RMS, and the so-called "off-axis sawteeth" (OAS)[12] are excited accordingly. Interestingly, the formation of ITBs and the excitation of RSAEs (or Alfvén cascades) take place concurrently when the off-axis minimum of safety factor ($q_{\min}$) is located at low-order rational surfaces ($q_{\min} = 1, 2, 3$).[13–15] The interaction between energetic ions and RSAEs is performed by hybrid MHD code,[16,17] which has attracted significant attention in magnetic fusion plasmas.[18–20] Therefore, the measurement of the distribution function of energetic ions density is more important for understanding of excitation of RSAEs and the establishment of ITBs.

The experiments are performed in Experimental Advanced Superconducting Tokamak (EAST), and the major and minor radius are $R \leq 1.9\,\mathrm{m}$ and $a \approx 0.45\,\mathrm{m}$, respectively. The energetic ions can be produced directly by the injection of neutral beam (NBI), and the two sources of NBI in the EAST Tokamak are deviated from the co-current direction with labels of NBI1L and NBI1R, respectively, as given in Fig. 1(a). The included angle between the beam lines of NBI1L and NBI1R is $\Delta\alpha \approx 8.7°$, and the beam lines of NBI1R are more perpendicular to the plasmas current than NBI1L. The neutral yield is dominated by interactions between the beam injected energetic ions and the thermal plasma,[21] namely the distribution of energetic ions can be speculated by the measurement of radial neutron camera (RNC).[22]

The RNC in EAST consists of a collimator and six liquid scintillators, which are located on the equatorial plane of port K, and the field of view are marked in Fig. 1(b). The points of tangency between the sightlines of RNC detectors with the poloidal magnetic surfaces are defined as $\rho_{\mathrm{rnc}}(r/a)$, e.g., the channel 2 with $\rho_{\mathrm{rnc}}(r/a) \approx 0.24$. Furthermore, the electron temperature T_{e} and line-integrated electron density $\langle n_{\mathrm{e}} \rangle$ are measured by the second harmonics mode of heterodyne radiometer of electron cyclotron emission (ECE) and Polarimeter Interferometer (POINT) arrays, respectively.

Supported by the National MCF Energy R&D Program of China (Grant Nos. 2019YFE03020000 and 2018YFE0304100), and the National Nature Science Foundation of China (Grant Nos. 11975267 and 11975273).
*Corresponding author. Email: gqzhong@ipp.ac.cn
© 2021 Chinese Physical Society and IOP Publishing Ltd

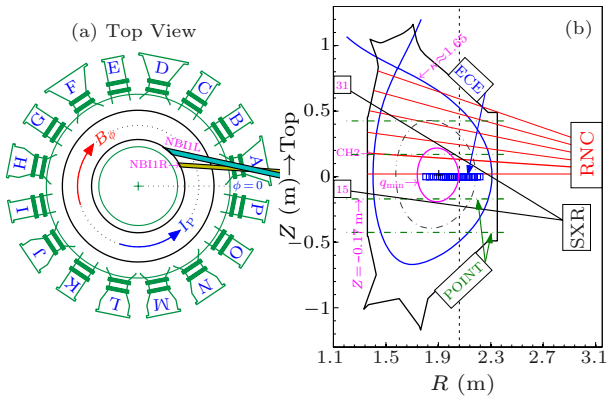

Fig. 1. Schematic diagrams of EAST top view (a) and side view (b). The injection directions of NBI1L and NBI1R are demonstrated in (a), and the layouts of partial diagnostics (radial positions of ECE, field of view of POINT, SXR and RNC) are given in (b).

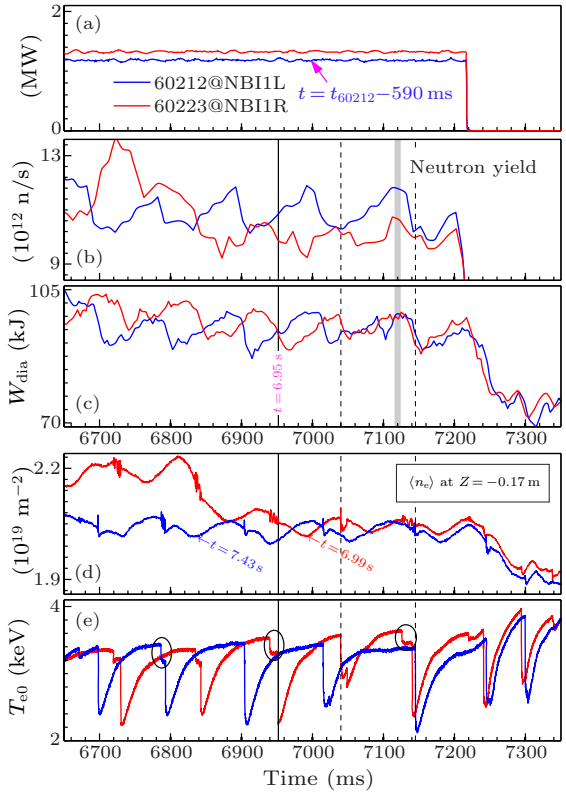

Fig. 2. Discharge conditions for two cases (60212→NBI1L & 60223→NBI1R). (a) Output power of NBI, (b) neutron yield f_n, (c) stored energy W_{dia}, (d) $\langle n_e\rangle$ measured by the POINT array at $Z=-0.17$ m, and (e) the core electron temperature T_{e0}. Note: the $\langle n_e\rangle$ of channel 60223 for $t\leq 6.85$ s is higher for the existence of ICRH as Ref. [23], which is switched off at $t\approx 6.8$ s.

The upper single null (USN) magnetic configuration is adopted with elongation $\kappa\approx 1.65$ at the last closed flux surface (LCFS) as shown in Fig. 1(b), and the safety factor is $q_{95}\approx 6.7$ at the 95% magnetic surface. The configuration of RMS is achieved by the combination of lower hybrid current driven (LHCD) and off-axis electron cyclotron resonance heating (ECRH), and the powers are $P_{LH}\geq 3$ MW and $P_{EC}\approx 0.5$ MW respectively. Two similar examples are selected as given in Fig. 2, and the time series of shot 60212 is moved forward for the convenient comparison ($t_{new}=t_{old}-590$ ms). The power P_{NB} and energy E_b for the two cases are nearly the same as $1.2\,\text{MW}\leq P_{NB}\leq 1.3\,\text{MW}$ and $E_b\approx 50$ keV respectively, while the injection directions of neutral beams are different (60212→NBI1L & 60223→NBI1R). Discharge parameters for the two cases are similar as follows: the neutron yield $f_n\approx 1\times 10^{13} n/s$, plasma stored energy $W_{dia}\approx 100$ kJ, core averaged ion temperature $T_{i0}\approx 1.5$ keV, and the maximum electron temperature and electron density are $T_{e0}\geq 3$ keV and $n_{e0}\geq 2.4\times 10^{19}$ m^{-3}, respectively.

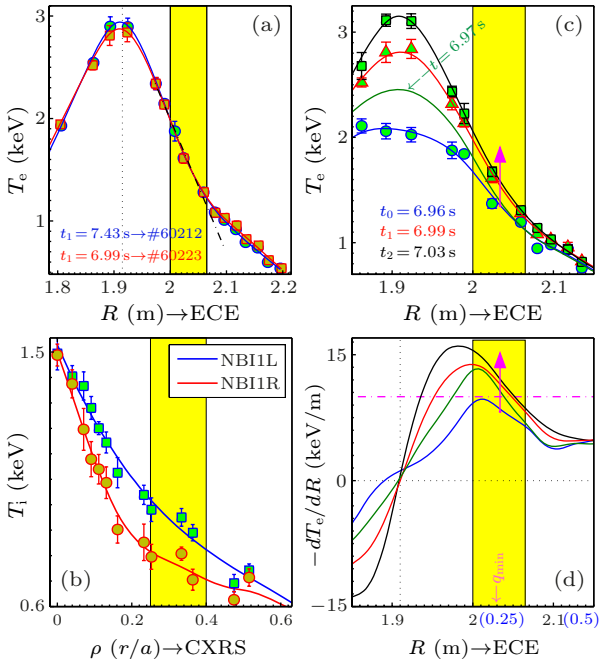

Fig. 3. Direct comparison of temperature profiles for the two cases. [(a), (b)] The profiles measured by ECE and CXRS arrays, respectively, and the alterations of T_e-profiles for shot 60223 are given in (c) and (d). Note: the position of q_{min} is filled by yellow color, and the normalized minor radius is marked by blue font in (d).

The two cases are compared and given as follows. Firstly, the OASs are reproduced periodically ($\tau_{OAS}\approx 100$ ms) for the two cases, and the alterations of W_{dia} and T_{e0} are $\Delta W_{dia}/W_{dia}\geq 10\%$ and $\Delta T_{e0}/T_{e0}\geq 30\%$, respectively. The excitation of precursor mode is accompanied by the minor collapse of core electron temperature, and the T_{e0} drops by 6% for the two cases as encompassed by the ellipses of Fig. 2(e). The precursor mode can be observed in the off-axis region $1.99\,\text{m}\leq R\leq 2.06\,\text{m}$ as described in Refs. [23,24], which is the reason for the title of "off-axis sawteeth". The mode number of the precursor mode is $m/n=2/1$, which is quite different in comparison with the conventional sawteeth of $m/n=1/1$, where the m and n are poloidal and toroidal num-

bers, respectively. Secondly, the T_e-profiles for the two cases are nearly the same as given in Fig. 3(a), and the stored energy is fully the same as shown in Fig. 2(c) for the moment of $t = 7.12$ s. Furthermore, the intensities of soft x-ray (SXR) signals for the two cases are fully the same, namely the plasma pressure can be expressed as $P \propto I_{sxr} \propto Z_{\rm eff} n_e^2 T_e^{-1/2}$. However, the T_i-profiles for two cases are slightly different as demonstrated in Fig. 3(b), which are measured by the charge exchange recombination spectroscopy (CXRS) for similar discharge conditions. Thirdly, the responses of energy and particles are discrete during the oscillation of OAS. The T_e restores swiftly after each collapse of OAS, while the thermal particles are transport outward persistently. The inflection point of electron density can be observed for each OAS oscillation, e.g., two moments ($t = 6.99\,{\rm s} \to 60223$ and $t = 7.43\,{\rm s} \to 60212$) are marked in Fig. 2, which means that the outward transport of thermal particles is suppressed subsequently. Fourthly, the threshold gradient of electron temperature is formed for each OAS. The steep gradient of electron temperature is formed for the inflection point of $\langle n_e \rangle$, and the confinement condition of thermal particles improves accordingly, where $|dT_e/dR|_{R\approx 2.05\,{\rm m}} \geq 10\,{\rm keV/m}$ is observed as shown in Fig. 3(d).

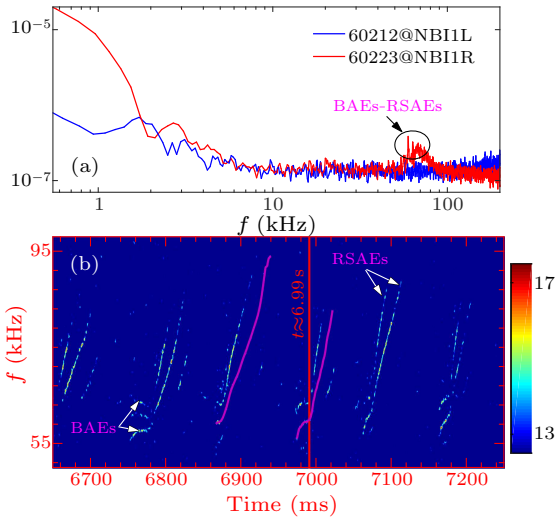

Fig. 4. The power spectra of ECE signal at the position of $q_{\rm min}$ for two cases are given in (a), and the frequency spectrogram of 60223 is given in (b).

However, the distribution functions of energetic ions densities for the two cases are different, and the neutron yield of shot 60223 is smaller than 60212 as given in Fig. 2(b). The RSAEs can be excited when the beam direction of NBI is switched from NBI1L to NBI1R, as shown in Fig. 4. The "grand cascade" is seen as a bunch of modes starting at the same time but with different frequencies, i.e., the pair of RSAEs with the same frequency but different n and m harmonics are excited simultaneously, and those branches are separated by the Doppler shifts. The eigenfrequency $\omega_{\rm RSAE}$ of RSAEs can be expressed as[7]

$$\omega_{\rm RSAE}^2 = \frac{v_{\rm A}^2}{R^2}\left(n - \frac{m}{q_{\rm min}}\right)^2 + \omega_{\rm BAE}^2 + \Delta\omega^2, \quad (1)$$

$$\frac{d}{dt}\omega_{\rm RSAE}(t) \approx m\frac{v_{\rm A}}{R}\frac{d}{dt}q_{\rm min}^{-1}(t), \quad (2)$$

where $v_{\rm A}$ is the Alfvén velocity, $\omega_{\rm BAE} \approx (2T_i/m_i)^{1/2} \times (7/4 + T_e/T_i)^{1/2}/R$ is the BAE angular frequency, and the $\Delta\omega$ term includes deviation from shear Alfvén continuum accumulation point due to, e.g., the corrections of fast ion pressure and finite pressure gradients. The minimum frequency $\omega_{\rm RSAE,min}$ in Eq. (1) can be set by BAE frequency for the conditions: the $q_{\rm min}$ takes on integral value ($q_{\rm min} = m/n$), and the $\Delta\omega$ term can be neglected for their small contributions. Each RSAE mode consists of predominantly one poloidal Fourier component, and the higher m has steeper slopes, as given by Eq. (2). The sloping rates ($k = df/dt$) of the above three adjacent branches are 0.5, 0.75 and 1 kHz/ms, respectively, as given in Ref. [23], namely the poloidal mode numbers m are $2l$, $3l$ and $4l$ respectively (l is integral number), where the branch of $m = 2l$ is marked by the magenta curves in Fig. 4(b).

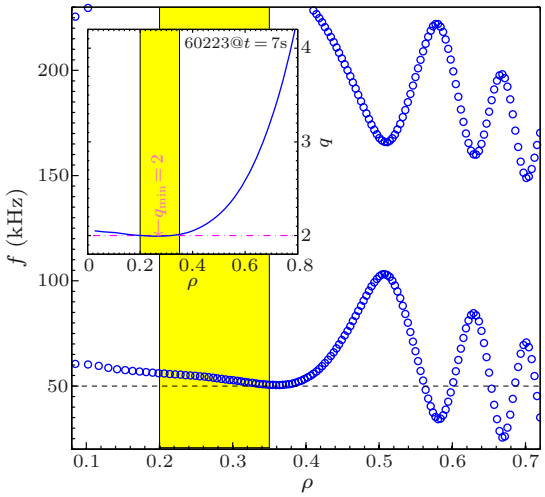

Fig. 5. The Alfvén continuum spectra with $n = 2$ is achieved by the weak magnetic shear q-profile ($q_{\rm min} \approx 2$).

The RSAEs can be transformed from the BAEs for the condition of $n - m/q_{\rm min} \neq 0$, and the upward sweeping frequency is observed for the decreasing $q_{\rm min}$ as given in Refs. [5,8,25]. One reasonable q-profile is reconstructed by the kinetic EFIT code as shown in Fig. 5, and the $q_{\rm min} \equiv 2$ is achieved for the existence of $m/n = 2/1$ precursor mode (where the estimation of $q_{\rm min} = 1$ is false in Refs. [23,24], which is misled by the disordered time series of SXR array). The minimum frequency of RSAE (or BAE) in the shaded region of $q_{\rm min}$ as demonstrated in Fig. 5 is nearly the same as experimental measurement. The

RSAE frequency starts from the BAE to the gap of toroidal Alfvén eigenmode (TAE), which is damped for the frequency $f \leq 95\,\text{kHz} < f_{\text{TAE}}$ [$\Delta f \leq 40\,\text{kHz}$, $f_{\text{TAE}} = v_{\text{A}}/(4\pi qR) \approx 120\,\text{kHz}$, $q = 2$]. The primary reason should be restricted by the lower energy of energetic ions, and the slowing down of beam ions $v_{\text{b,s}} < v_{\text{b,max}} \approx 2.2 \times 10^6\,\text{m/s}$, $v_{\text{A}} \approx 6 \times 10^6\,\text{m/s}$.

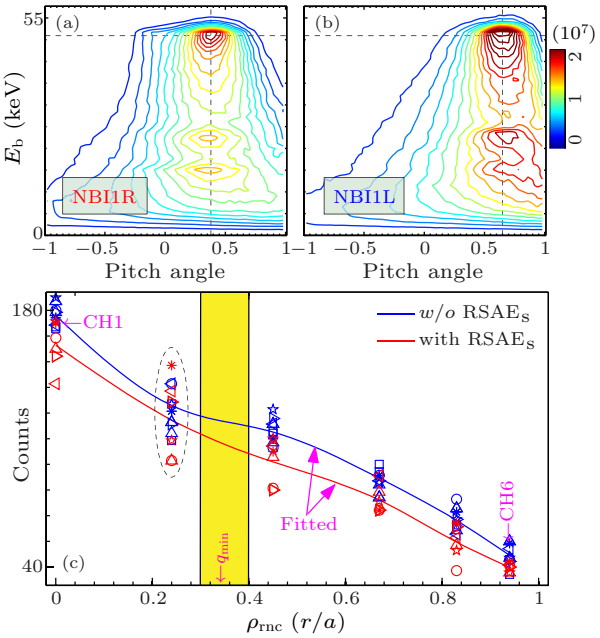

Fig. 6. Profiles of energetic ions: (a) and (b) are classical distributions in the velocity space achieved by simulation, and the energetic ions density are measured by RNC as given in (c).

The distribution function of energetic ions density with plasma equilibria using the guiding center code ORBIT and NUBEAM/TRANSP has been performed in EAST as described in Ref. [26] and demonstrated in Figs. 6(a) and 6(b). The initial beam energy is $E_{\text{b}} \approx 50\,\text{keV}$, and the pitch angles $(v_{\parallel}/v)$ of beam NBI1R is smaller than the beam NBI1L, which are $v_{\parallel}/v \sim 0.38$ and $v_{\parallel}/v \sim 0.65$, respectively. The slowing-down beam ion density distribution profiles of the two beams (NBI1L and NBI1R) are measured by the RNC, as given in Fig. 6(c). The gradient of energetic ions densities for the case 60223 (NBI1R) is steeper than the case 60212 (NBI1L) in the region of $q_{\min}$, which is further confirmed by the measurements of T_{i}-profiles, where the flattened region of the case 60212 may be caused by the poor spatial resolution of RNC array. The excitation condition of RSAEs can be expressed as

$$\frac{\gamma}{\omega_r} \propto n_{\text{E}} \left(\frac{\omega_{*,\text{E}}}{\omega} - 1\right) \{\delta[\omega - (nq_{\min} - m + 1)v_{\parallel}] + \delta[\omega - (nq_{\min} - m - 1)v_{\parallel}]\},$$

where n_{E} is the energetic ions density, $\omega_{*,\text{E}} = -T_{\text{i}} k_\theta \partial_r \ln f_{0,\text{E}}/(Be)$ is the diamagnetic drift frequency of energetic ions, accounting for free energy from energetic ions nonuniformity, $f_{0,\text{E}}$ is the distribution function of energetic ions density. Therefore, a pair of RSAEs are excited easily when the beam of NBI1R (perpendicular) is adopted.

In conclusion, the excitation conditions of RSAEs have been investigated on the EAST tokamak during the oscillation of OAS. The basic features of the OAS for the two cases (60212→NBI1L & 60223→NBI1R) are similar in the configuration of RMS, and the outward transport of thermal particles is suppressed for the formation of threshold gradient of electron temperature in the vicinity of $q_{\min}$. The core steep gradient of energetic ions density is formed when the perpendicular injection of NBI (NBI1R) is selected, and a pair of RSAEs are excited accordingly. Furthermore, the formation of threshold gradient of electron temperature and the excitation of RSAEs take place concurrently, which means that the neutral beam with perpendicular injection (NBI1R) is beneficial for the establishment of internal transport barrier that has been testified in the EAST campaigns.

References

[1] Ida K and Fujita T 2018 *Plasma Phys. Control. Fusion* **60** 033001

[2] Strait E J, Lao L L, Mauel M E, Rice B W, Taylor T S, Burrell K H, Chu M S, Lazarus E A, Osborne T H, Thompson S J and Turnbull A D 1995 *Phys. Rev. Lett.* **75** 4421

[3] Levinton F M, Zarnstorff M C, Batha S H, Bell M, Bell R E, Budny R V, Bush C, Chang Z, Fredrickson E, Janos A, Manickam J, Ramsey A, Sabbagh S A, Schmidt G L, Synakowski E J and Taylor G 1995 *Phys. Rev. Lett.* **75** 4417

[4] Heidbrink W W 2008 *Phys. Plasmas* **15** 055501

[5] Berk H L, Borba D N, Breizman B N, Pinches S D and Sharapov S E 2001 *Phys. Rev. Lett.* **87** 185002

[6] Deng W, Lin Z, Holod I, Wang Z, Xiao Y and Zhang H 2012 *Nucl. Fusion* **52** 043006

[7] Breizman B N and Sharapov S E 2011 *Plasma Phys. Control. Fusion* **53** 054001

[8] Chen W, Yu L, Liu Y, Ding X T, Xie H S, Zhu J, Yu L M, Ji X Q, Li J X, Li Y G, Yu D L, Shi Z B, Song X M, Cao J Y, Song S D, Dong Y B, Zhong W L, Jiang M, Cui Z Y, Huang Y, Zhou Y, Dong J Q, Xu M, Xia F, Yan L W, Yang Q W, Duan X R and the H L A T 2014 *Nucl. Fusion* **54** 104002

[9] Wang Z, Wang X, Dong J, Lei Y, Long Y, Mou Z and Qu W 2007 *Phys. Rev. Lett.* **99** 185004

[10] Wei L and Wang Z X 2014 *Nucl. Fusion* **54** 043015

[11] Zhang W, Ma Z W, Zhu J and Zhang H W 2019 *Plasma Phys. Control. Fusion* **61** 075002

[12] Chang Z, Park W, Fredrickson E D, Batha S H, Bell M G, Bell R, Budny R V, Bush C E, Janos A, Levinton F M, McGuire K M, Park H, Sabbagh S A, Schmidt G L, Scott S D, Synakowski E J, Takahashi H, Taylor G and Zarnstorff M C 1996 *Phys. Rev. Lett.* **77** 3553

[13] Joffrin E, Challis C D, Conway G D, Garbet X, Gude A, Günter S, Hawkes N C, Hender T C, Howell D F, Huysmans G T A, Lazzaro E, Maget P, Marachek M, Peeters A G, Pinches S D, Sharapov S E and JET-EFDA contributors 2003 *Nucl. Fusion* **43** 1167

[14] Sharapov S E, Alper B, Yu F B, Berk H L, Borba D, Boswell C, Breizman B N, Challis C D, Baar M D, Luna E D L, Evangelidis E A, Hacquin S, Hawkes N C, Kiptily V G, Pinches S D, Sandquist P, Voitsekhovich I, Young N P and JET-EFDA contributors 2006 *Nucl. Fusion* **46** S868
[15] Austin M E, Burrell K H, Waltz R E, Gentle K W, Gohil P, Greenfield C M, Groebner R J, Heidbrink W W, Luo Y, Kinsey J E, Makowski M A, McKee G R, Nazikian R, Petty C C, Prater R, Rhodes T L, Shafer M W and Zeeland M A V 2006 *Phys. Plasmas* **13** 082502
[16] Yang Y R, Chen W, Ye M Y, Yuan J B and Xu M 2020 *Nucl. Fusion* **60** 106012
[17] Wang T, Qiu Z, Zonca F, Briguglio S and Vlad G 2020 *Nucl. Fusion* **60** 126032
[18] Chen L and Zonca F 2016 *Rev. Mod. Phys.* **88** 015008
[19] Todo Y 2019 *Rev. Mod. Plasma Phys.* **3** 1
[20] Chen L, Zonca F and Lin Y 2021 *Rev. Mod. Plasma Phys.* **5** 1
[21] Sharapov S, Alper B, Berk H, Borba D, Breizman B, Challis C, Classen I, Edlund E, Eriksson J, Fasoli A, Fredrickson E, Fu G, Garcia-Munoz M, Gassner T, Ghantous K, Goloborodko V, Gorelenkov N, Gryaznevich M, Hacquin S, Heidbrink W, Hellesen C, Kiptily V, Kramer G, Lauber P, Lilley M, Lisak M, Nabais F, Nazikian R, Nyqvist R, Osakabe M, Thun C P V, Pinches S, Podesta M, Porkolab M, Shinohara K, Schoepf K, Todo Y, Toi K, Zeeland M V, Voitsekhovich I, White R, Yavorskij V, TG I E and JET-EFDA contributors 2013 *Nucl. Fusion* **53** 104022
[22] Zhong G, Hu L Q, Pu N, Zhou R J, Xiao M, Cao H R, Zhu Y B, Li K, Fan T S, Peng X Y, Du T F, Ge L J, Huang J, Xu G S, Wan B N and Team E 2016 *Rev. Sci. Instrum.* **87** 11D820
[23] Xu M, Zhao H L, Zang Q, Zhong G Q, Xu L Q, Liu H Q, Chen W, Huang J, Hu L Q, Xu G S, Gong X Z, Qian J P, Liu Y, Zhang T, Zhang Y, Sun Y W, Zhang X D and Wan B N 2019 *Nucl. Fusion* **59** 084005
[24] Xu M, Zhao H L, Zhang J Z, Xu L Q, Liu H Q, Li G Q, Zhong G Q, Zang Q, Hu L Q, Gong X Z, Xu G S, Zhang X D, Wan B N and team EAST 2020 *Nucl. Fusion* **60** 112005
[25] Edlund E M, Porkolab M, Kramer G J, Lin L, Lin Y and Wukitch S J 2009 *Phys. Rev. Lett.* **102** 165003
[26] Wu B, Hao B, White R, Wang J, Zang Q, Han X and Hu C 2016 *Plasma Phys. Control. Fusion* **59** 025004